

ORIGINAL RESEARCH

# Diabetes and Excess Aldosterone Promote Heart Failure With Preserved Ejection Fraction

Bence Hegyi , MD, PhD; Juliana Mira Hernandez , DVM, PhD; Christopher Y. Ko , PhD; Junyoung Hong , PhD; Erin Y. Shen, BS; Emily R. Spencer , BS; Daria Smoliarchuk, BS; Manuel F. Navedo , PhD; Donald M. Bers , PhD; Julie Bossuyt , DVM, PhD

**BACKGROUND:** The pathobiology of heart failure with preserved ejection fraction (HFpEF) is still poorly understood, and effective therapies remain limited. Diabetes and mineralocorticoid excess are common and important pathophysiological factors that may synergistically promote HFpEF. The authors aimed to develop a novel animal model of HFpEF that recapitulates key aspects of the complex human phenotype with multiorgan impairments.

**METHODS AND RESULTS:** The authors created a novel HFpEF model combining leptin receptor–deficient *db/db* mice with a 4-week period of aldosterone infusion. The HFpEF phenotype was assessed using morphometry, echocardiography,  $Ca^{2+}$  handling, and electrophysiology. The sodium-glucose cotransporter-2 inhibitor empagliflozin was then tested for reversing the arrhythmogenic cardiomyocyte phenotype. Continuous aldosterone infusion for 4 weeks in *db/db* mice induced marked diastolic dysfunction with preserved ejection fraction, cardiac hypertrophy, high levels of B-type natriuretic peptide, and significant extracardiac comorbidities (including severe obesity, diabetes with marked hyperglycemia, pulmonary edema, and vascular dysfunction). Aldosterone or *db/db* alone induced only a mild diastolic dysfunction without congestion. At the cellular level, cardiomyocyte hypertrophy, prolonged  $Ca^{2+}$  transient decay, and arrhythmogenic action potential remodeling (prolongation, increased short-term variability, delayed afterdepolarizations), and enhanced late  $Na^+$  current were observed in aldosterone-treated *db/db* mice. All of these arrhythmogenic changes were reversed by empagliflozin pretreatment of HFpEF cardiomyocytes.

**CONCLUSIONS:** The authors conclude that the *db/db*+aldosterone model may represent a distinct clinical subgroup of HFpEF that has marked hyperglycemia, obesity, and increased arrhythmia risk. This novel HFpEF model can be useful in future therapeutic testing and should provide unique opportunities to better understand disease pathobiology.

**Key Words:** arrhythmia ■ diabetes ■ HFpEF ■ mineralocorticoid ■ SGLT2 inhibitor

**H**eat failure with preserved ejection fraction (HFpEF) is a critical and unresolved public health concern because of its increasing prevalence, high morbidity and mortality, and limited clinical treatment options.<sup>1</sup> In addition to the characteristic diastolic dysfunction and common extracardiac comorbidities (eg, hypertension, diabetes, obesity, exercise intolerance, lung and kidney diseases), patients with HFpEF have longer QTc<sup>2</sup> and increased incidence of nonsustained ventricular

tachycardia on ambulatory ECGs.<sup>2,3</sup> The risk for cardiac arrhythmias and sudden cardiac death may also be increased in HFpEF,<sup>4,5</sup> especially in patients with insulin-treated diabetes.<sup>6</sup> Importantly, almost all drugs that provide benefit in patients with heart failure with reduced ejection fraction (EF) have failed clinical trials in HFpEF, with exceptions being the mineralocorticoid receptor antagonist spironolactone<sup>7</sup> and the sodium-glucose cotransporter-2 (SGLT2) inhibitors empagliflozin<sup>8</sup> and

Correspondence to: Julie Bossuyt, DVM, PhD, and Bence Hegyi, MD, PhD, Department of Pharmacology, University of California, Davis, 451 Health Sciences Drive, Davis, CA 95616. Email: [jbossuyt@ucdavis.edu](mailto:jbossuyt@ucdavis.edu); [bhegyi@ucdavis.edu](mailto:bhegyi@ucdavis.edu)

Supplemental Material is available at <https://www.ahajournals.org/doi/suppl/10.1161/JAHA.122.027164>

For Sources of Funding and Disclosures, see page 11.

© 2022 The Authors. Published on behalf of the American Heart Association, Inc., by Wiley. This is an open access article under the terms of the [Creative Commons Attribution-NonCommercial-NoDerivs](https://creativecommons.org/licenses/by-nc-nd/4.0/) License, which permits use and distribution in any medium, provided the original work is properly cited, the use is non-commercial and no modifications or adaptations are made.

JAHA is available at: [www.ahajournals.org/journal/jaha](http://www.ahajournals.org/journal/jaha)

## CLINICAL PERSPECTIVE

### What Is New?

- Diabetes and mineralocorticoid excess are synergistic pathogenic factors in promoting heart failure with preserved ejection fraction (HFpEF) phenotype.
- Diabetes and aldosterone induce diastolic Ca<sup>2+</sup> handling impairments and action potential duration prolongation and enhance late Na<sup>+</sup> current, which promote diastolic dysfunction and arrhythmias in HFpEF.
- The sodium-glucose cotransporter-2 inhibitor empagliflozin reverses action potential duration prolongation and late Na<sup>+</sup> current enhancement, acting directly on HFpEF cardiomyocytes.

### What Are the Clinical Implications?

- Patients with HFpEF and diabetic hyperglycemia may exhibit more severe diastolic dysfunction and have increased arrhythmia risk.
- Patients with HFpEF and diabetes may benefit from drugs targeting mineralocorticoid signaling.
- The sodium-glucose cotransporter-2 inhibitor empagliflozin may have an important beneficial effect on cardiac electrical activity in patients with HFpEF and diabetic cardiomyopathy.

## Nonstandard Abbreviations and Acronyms

<b>AP</b>	action potential
<b>db/db+Aldo</b>	<i>db/db</i> mice infused with aldosterone
<b>APD</b>	action potential duration
<b>CaT</b>	Ca <sup>2+</sup> transient
<b>db/db</b>	leptin receptor-deficient mice ( <i>Lep<sup>r</sup>-db/db</i> )
<b>HFpEF</b>	heart failure with preserved ejection fraction
<b>I<sub>Na,Late</sub></b>	late Na <sup>+</sup> current
<b>L-NAME</b>	N <sup>ω</sup> -nitro-L-arginine methyl ester
<b>SGLT2</b>	sodium-glucose cotransporter-2
<b>SR</b>	sarcoplasmic reticulum
<b>WT</b>	wild-type

dapagliflozin.<sup>9</sup> However, further randomized HFpEF clinical trials are needed, and the exact molecular mechanisms of cardioprotective effects of these drugs remain incompletely understood.<sup>10</sup> Therefore, there is a pressing unmet need for better understanding of the disease pathophysiology and identification of novel therapeutic targets.

Progress in understanding and treating HFpEF has been hampered by limitations in preclinical animal models for HFpEF that fail to represent the full spectrum of the complex, multiorgan human HFpEF phenotype.<sup>11</sup> Moreover, multiple models may be needed to capture the clinically heterogeneous human HFpEF patient population.<sup>1,12,13</sup> Recently, 2- or multi-hit models emerged to more closely recapitulate the human HFpEF syndrome.<sup>11</sup> These models include high-fat diet-fed mice treated with the constitutive nitric oxide synthase inhibitor N<sup>ω</sup>-nitro-L-arginine methyl ester (L-NAME),<sup>14</sup> ZSF1 diabetic plus spontaneously hypertensive rats treated with the vascular endothelial growth factor-2 inhibitor SU5416,<sup>15</sup> western diet-fed and aortic-banded pigs,<sup>16</sup> and western diet-fed pigs treated with excess mineralocorticoid (deoxycorticosterone acetate).<sup>17</sup> Topical reviews highlighted that in addition to these multi-hit models, the leptin receptor-deficient *db/db* and aldosterone infusion models can each recapitulate human HFpEF to a certain degree.<sup>10,18</sup> However, *db/db*<sup>19,20</sup> or aldosterone infusion<sup>21</sup> alone may not induce severe diastolic dysfunction or multiorgan HFpEF phenotype. Here, we introduce a novel murine HFpEF model in which *db/db* mice are chronically infused with aldosterone (*db/db*+Aldo mice), thus combining marked metabolic alteration with mineralocorticoid excess. We hypothesized that this combination may synergize, leading to a robust HFpEF phenotype with marked diastolic dysfunction, increased proarrhythmia risk, and significant systemic multiorgan impairments. This model would complement the existing HFpEF models in having a more diabetic phenotype, because a one-size-fits-all therapeutic strategy is unlikely to work in HFpEF.<sup>1</sup> Patients with diabetic HFpEF represent a large clinical pheno-subgroup<sup>22</sup> with distinct myocardial gene expression profile,<sup>23</sup> impaired cardiomyocyte Ca<sup>2+</sup> homeostasis,<sup>24</sup> and a particularly poor prognosis but better response to spironolactone therapy<sup>22</sup> compared with patients with nondiabetic HFpEF.

Here we show that *db/db* and chronic aldosterone infusion separately induced only very mild diastolic dysfunction without pulmonary congestion in mice. However, when these 2 factors are combined, *db/db*+Aldo mice exhibit marked diastolic dysfunction with preserved EF, cardiac hypertrophy, high levels of B-type natriuretic peptide (BNP), and significant extracardiac comorbidities (morbid obesity, diabetes with marked hyperglycemia, pulmonary edema, and vascular dysfunction) in line with current human HFpEF diagnostic criteria.<sup>11</sup> At the cellular level, cardiomyocyte hypertrophy, prolonged Ca<sup>2+</sup> transient (CaT) decay, and arrhythmogenic action potentials (APs) were observed in *db/db*+Aldo mice. Empagliflozin reversed the late Na<sup>+</sup> current (*I<sub>Na,Late</sub>*) enhancement and proarrhythmic AP changes in *db/db*+Aldo, directly acting on cardiomyocytes despite that cardiomyocytes lack SGLT2

expression,<sup>25</sup> providing additional insights into myocyte drug targets and therapeutic benefits of empagliflozin. In conclusion, the *db/db*+Aldo model can be an important translational murine model of a more diabetic phenotype to complement existing animal models for studying disease pathobiology and future therapeutic testing in HFpEF.

## METHODS

All animal handling and laboratory procedures were in accordance with the approved protocols (#21572 and 22834) of the Institutional Animal Care and Use Committee at University of California, Davis, conforming to the *National Institutes of Health Guide for the Care and Use of Laboratory Animals* (8th edition, 2011).

The data underlying this article will be shared on reasonable request to the corresponding authors.

Detailed methods are available in Data S1.

### Animal Procedures

Twenty-four adult (10-week-old, both sexes) *Lepr<sup>db/db</sup>* (stock #000697) and 24 corresponding wild-type (WT) mice on C57BL6/J background were obtained from Jackson Laboratory. The animals were kept at standard temperature, humidity, and lighting. Food (Teklad, 2018) and drinking water were provided ad libitum. Osmotic minipumps (Alzet, model 2004) that delivered a continuous infusion of either d-aldosterone (0.3  $\mu\text{g}/\text{h}$ )<sup>21</sup> or vehicle (saline with 5% ethanol) for 4 weeks were implanted subcutaneously in 12-week-old mice (Figure 1A). We used block randomization with a block size of 4 animals (for 1 genotype and treatment group in 1 sex), with 16 control (WT+vehicle) and 16 two-hit (*db/db*+Aldo) mice included (allowing for detailed isolated myocyte studies), and for the one-hit controls we used 8 WT+Aldo and 8 *db/db*+vehicle mice. For proper allocation concealment, animals were recruited blinded based on sequential ear tag numbers randomly assigned by the animal housing facility. Each treatment group included an equal number of male and female animals. Enzymatic isolation of left ventricular (LV) cardiomyocytes was performed as previously described.<sup>26</sup>

### Blood Glucose, Aldosterone, and BNP Measurements

Blood glucose levels were measured in fresh blood samples collected from the middle tail vein using OneTouch UltraMini blood glucose monitoring system and test strips (LifeScan). BNP and aldosterone levels were measured in blood plasma by ELISA using manufacturers' instructions (RayBiotech, EIAM-BNP-1 and Cayman Chemical, Aldosterone EIA, respectively). Three technical replicates were performed for each biological sample.

## Arterial Diameter Measurements

Freshly isolated mesenteric artery segments were mounted in a 5-mL myograph chamber to determine arterial diameter changes in response to changes in intraluminal pressure as previously described.<sup>27</sup>

## Echocardiography

Transthoracic echocardiography was performed in anesthetized (isoflurane, 1%–3%) animals. LV M-mode and Doppler images were acquired using a Vevo 2100 echocardiography system (FUJIFILM VisualSonics) equipped with a 40-MHz transducer. Body temperature was carefully monitored, and anesthesia was adjusted to achieve heart rates of 350 to 450 beats per minute to assess diastolic dysfunction and 450 to 600 beats per minute to assess systolic cardiac function in each animal.

## Calcium Imaging

Intracellular CaTs were measured using confocal microscopy in freshly isolated ventricular cardiomyocytes loaded with Fluo-4 AM (10  $\mu\text{mol}/\text{L}$ , 30 minutes; Invitrogen) at room temperature.<sup>26</sup>

## Cellular Electrophysiology

APs were recorded in isolated ventricular cardiomyocytes using patch-clamp with physiological solutions at 37 °C.<sup>26</sup> Arrhythmogenic diastolic activities were assessed during a 1-minute period following cessation of tachypacing. In voltage-clamp experiments,  $I_{\text{Na,Late}}$  was measured using 500-millisecond depolarizing voltage pulses to  $-40\text{mV}$  from  $-120\text{mV}$  holding potential in every 5 seconds.

## Statistical Analysis

Data are presented as mean $\pm$ SEM. Statistical significance of differences was determined using *t* test, Mann–Whitney test, and ANOVA followed by Tukey or Dunn multiple comparisons test, when applicable. GraphPad Prism 9 was used for data analysis.  $P < 0.05$  was considered statistically significant.

## RESULTS

### Diabetes and Aldosterone Excess Induce Multiorgan Impairments Characteristic of HFpEF

Figure 1A illustrates the *db/db*+Aldo mouse protocol and measurements made at the end of 4-week continuous aldosterone (or vehicle) infusion. Plasma aldosterone levels were elevated 2.5-fold following 4-week aldosterone infusion (versus vehicle) in both WT and *db/db* mice (Figure 1B). Morphometric evaluations (Figure 1C) showed morbid obesity, marked

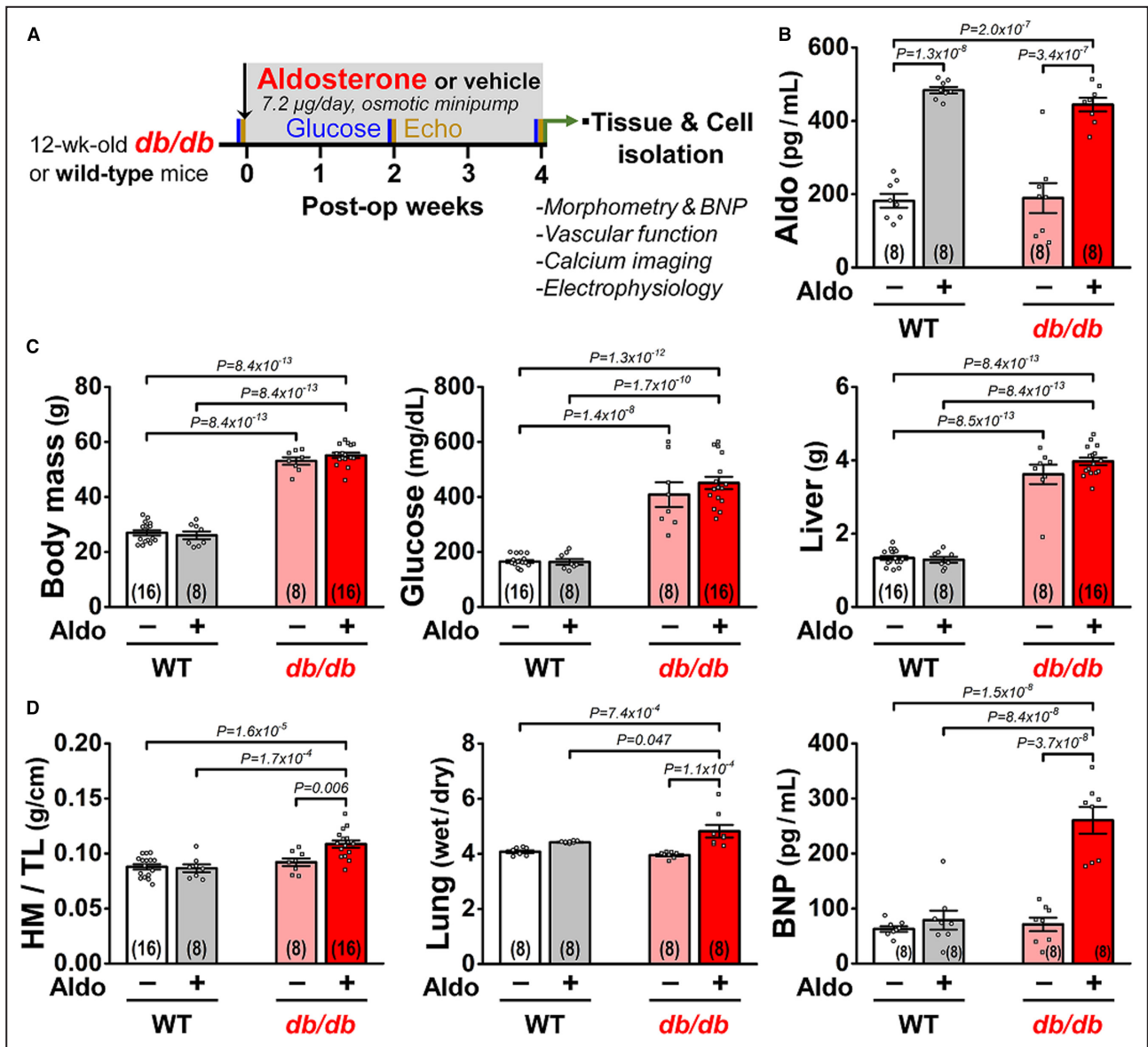


**Figure 1. Robust heart failure with preserved ejection fraction (HFpEF) phenotype in *db/db* mice with chronic aldosterone infusion.**

**A**, Study protocol of HFpEF-inducing treatment and assessment of cardiac function and multiorgan impairments. **B**, Plasma aldosterone levels 4 weeks after osmotic minipump implantation in WT and leptin receptor-deficient *db/db* mice. **C**, Marked obesity, hyperglycemia, and hepatomegaly in *db/db* mice. **D**, Cardiac hypertrophy, pulmonary edema, and high BNP plasma levels in *db/db*+Aldo. Mean±SEM is shown. ANOVA followed by Tukey multiple comparisons test. Animal numbers are shown in the figure. BNP indicates B-type natriuretic peptide; *db/db*+Aldo, *db/db* mice with chronic aldosterone infusion; HFpEF, heart failure with preserved ejection fraction; HM/TL, heart mass to tibia length ratio; and WT, wild-type.

hyperglycemia, and hepatomegaly in all *db/db* mice (independent of aldosterone infusion) as expected in this genotype. However, only *db/db*+Aldo mice exhibited significant cardiac hypertrophy ( $P=0.011$  for interaction between *db/db* genotype and aldosterone treatment in 2-way ANOVA), pulmonary edema ( $P=0.037$ ), and elevated BNP levels ( $P=1.2 \times 10^{-5}$ ) as shown in Figure 1D. No major morphometric alteration was observed in aldosterone-treated WT mice (WT+Aldo) versus vehicle-treated WT controls (WT+vehicle).

### Diabetes and Aldosterone Excess Induce Vascular Remodeling in HFpEF

Extracardiac comorbidities, including vascular abnormalities (vascular stiffening and endothelial and microvascular dysfunction) and hypertension, are frequently reported in patients with HFpEF. We carefully measured the arterial diameters and the myogenic response over a range of intravascular pressures (10 to 100 mmHg) in isolated mesenteric arteries in WT+vehicle

and *db/db*+Aldo mice (Figure 2A). Significant vascular remodeling in *db/db*+Aldo mice was evident from markedly increased myogenic tone (Figure 2B), which could contribute to an increased mechanical afterload on the heart.

### *db/db*+Aldo Mice Exhibit Marked Diastolic Dysfunction and Preserved EF

Echocardiographic evaluation (Figure 3) showed preserved fractional shortening and EF in WT+Aldo mice, whereas contractility was slightly reduced in *db/db*+vehicle mice. Importantly, fractional shortening and EF were preserved in *db/db*+Aldo mice (Figure 3A and 3B). Moreover, *db/db*+Aldo hearts exhibited significant concentric hypertrophy quantified as LV remodeling index (a ratio between LV mass/LV end-diastolic internal diameter;  $P=1.2 \times 10^{-5}$  for interaction between *db/db* and Aldo), whereas *db/db*+vehicle hearts showed only a small tendency for LV hypertrophy, and LV remodeling index was unchanged in WT+Aldo (Figure 3B). Indices of diastolic dysfunction (mitral *E/A* and *E/e'*) progressively increased during chronic aldosterone infusion (Figure S1), and, by the end of 4-week treatment, both measures (Figure 3C) were markedly increased in *db/db*+Aldo mice (*E/e'*,  $P=1.6 \times 10^{-8}$  for interaction between *db/db* and Aldo). In contrast, *db/db*+vehicle and WT+Aldo mice only showed slight increases in *E/A* and *E/e'* over the 4-week study period versus WT+vehicle (Figure 3C; Figure S2). Left atrial (LA) enlargement is a marker of diastolic dysfunction,<sup>28</sup> frequently observed in patients with HFpEF,<sup>29</sup> and LA area was also significantly increased in *db/db*+Aldo mice ( $P=0.001$  for interaction between *db/db* and Aldo) but only slightly increased in *db/db*+vehicle and WT+Aldo mice (Figure 3C). These data suggest a synergy between

diabetes and aldosterone signaling in promoting diastolic dysfunction.

### *db/db*+Aldo Mice Exhibit Diastolic Impairments in Cardiomyocyte Calcium Handling

Impaired cardiomyocyte  $\text{Ca}^{2+}$  handling can promote contractile dysfunction and arrhythmias.<sup>30,31</sup> Intracellular CaTs in *db/db*+Aldo myocytes stimulated at 1 Hz exhibited unchanged peak  $[\text{Ca}^{2+}]_i$ , elevated diastolic  $[\text{Ca}^{2+}]_i$ , and slowed decline of CaTs indicative of slower sarcoplasmic reticulum (SR)  $\text{Ca}^{2+}$  reuptake (Figure 4A through 4C). The elevated diastolic  $[\text{Ca}^{2+}]_i$  caused by slower CaT decline results in a trend toward smaller CaT amplitude. However, the caffeine-induced CaT amplitude was unchanged, indicating similar SR  $\text{Ca}^{2+}$  content in *db/db*+Aldo versus control myocytes (Figure 4C).

### *db/db*+Aldo Murine Cardiomyocytes Have Proarrhythmogenic Electrophysiological Changes

Because arrhythmias are more frequent in diabetic patients with HFpEF, we tested for proarrhythmic remodeling in *db/db*+Aldo mice. AP duration (APD) was markedly prolonged in *db/db*+Aldo mice (Figure 5A). APD prolongation was prominent at the later phase of repolarization (75% and 90% of repolarization) (Figures 5A; Figure S3). Moreover, short-term temporal variability of APD was also markedly increased in *db/db*+Aldo (Figure 5B), which may reflect increased spontaneous  $\text{Ca}^{2+}$  release.<sup>26,32</sup> To further assess arrhythmia susceptibility, we tested spontaneous diastolic activities following a tachypacing protocol (1 minute at 10 Hz pacing). Delayed afterdepolarizations

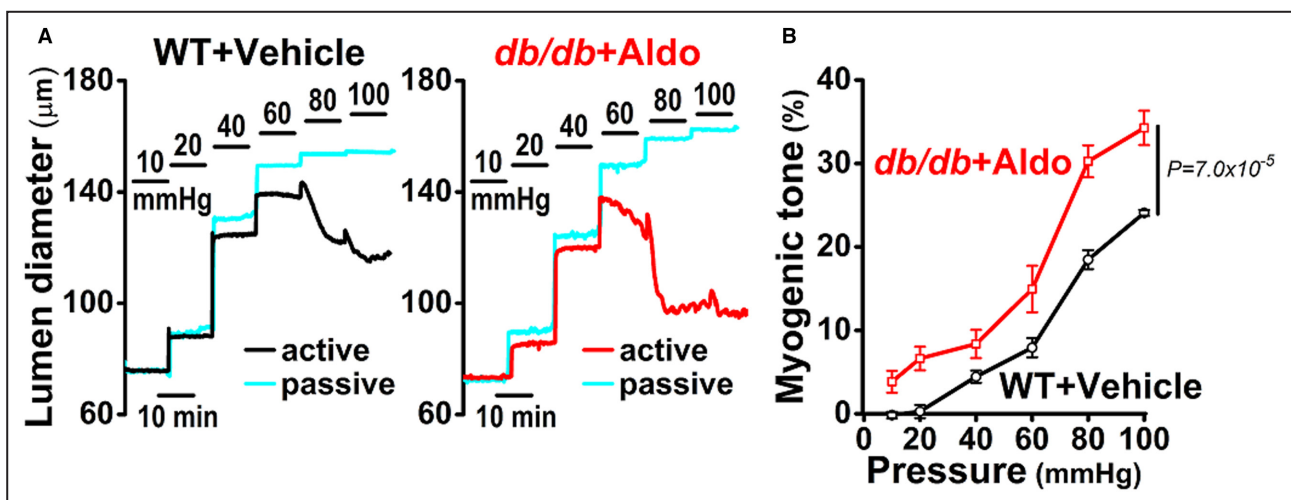


**Figure 2.** Impaired arterial function in *db/db* mice with chronic aldosterone infusion.

A, Increased arterial myogenic tone in *db/db*+Aldo ( $n=7$  arteries from 5 animals) vs WT mice with vehicle infusion (WT+vehicle,  $n=5$  arteries from 5 animals). Mean $\pm$ SEM is shown. Two-way repeated measures ANOVA with Geisser–Greenhouse correction. *db/db*+Aldo indicates *db/db* mice with chronic aldosterone infusion; and WT, wild-type.

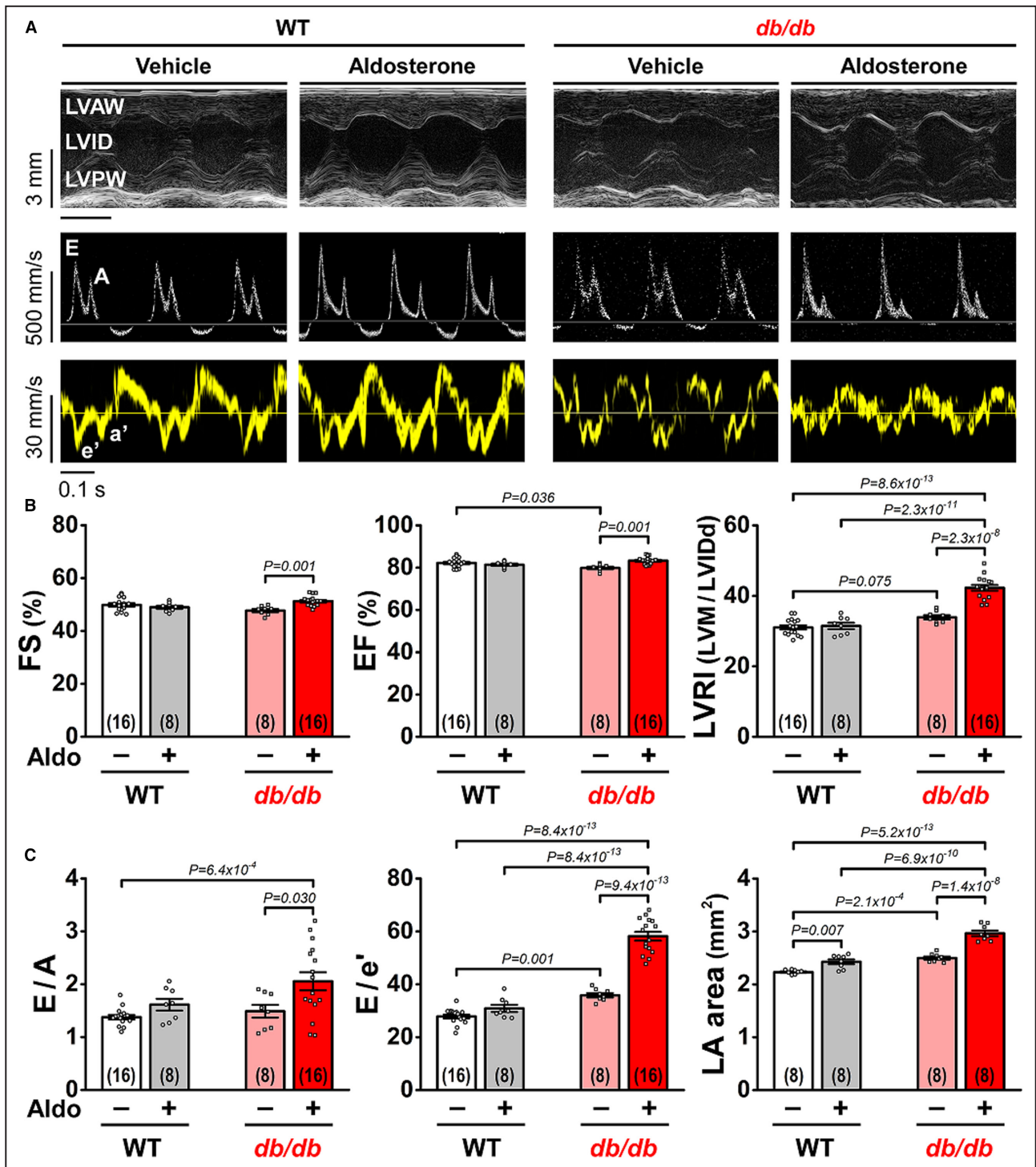


**Figure 3. Marked diastolic dysfunction with preserved systolic function in *db/db*+*db*+Aldo.**

**A**, Representative LV M-mode, flow, and tissue Doppler echocardiographic images 4 weeks after aldosterone or vehicle minipump implantation in WT and *db/db* mice. **B**, Preserved FS and EF, and significantly increased LVRI in *db/db*+Aldo. **C**, Severe diastolic dysfunction and LA enlargement in *db/db*+Aldo. Mean±SEM is shown. ANOVA followed by Tukey multiple comparisons test. Animal numbers are shown in the figure. *db/db*+Aldo indicates *db/db* mice with chronic aldosterone infusion; *E/A*, ratio between mitral *E* wave and *A* wave; *E/e'*, ratio between mitral *E* wave and *e'* wave; EF, ejection fraction; FS, fractional shortening; LA, left atrial; LV, left ventricular; LVAW, left ventricular anterior wall; LVID, left ventricular internal diameter; LVIDd, end-diastolic left ventricular internal diameter; LVM, left ventricular mass; LVPW, left ventricular posterior wall; LVRI, LV remodeling index; and WT, wild-type.

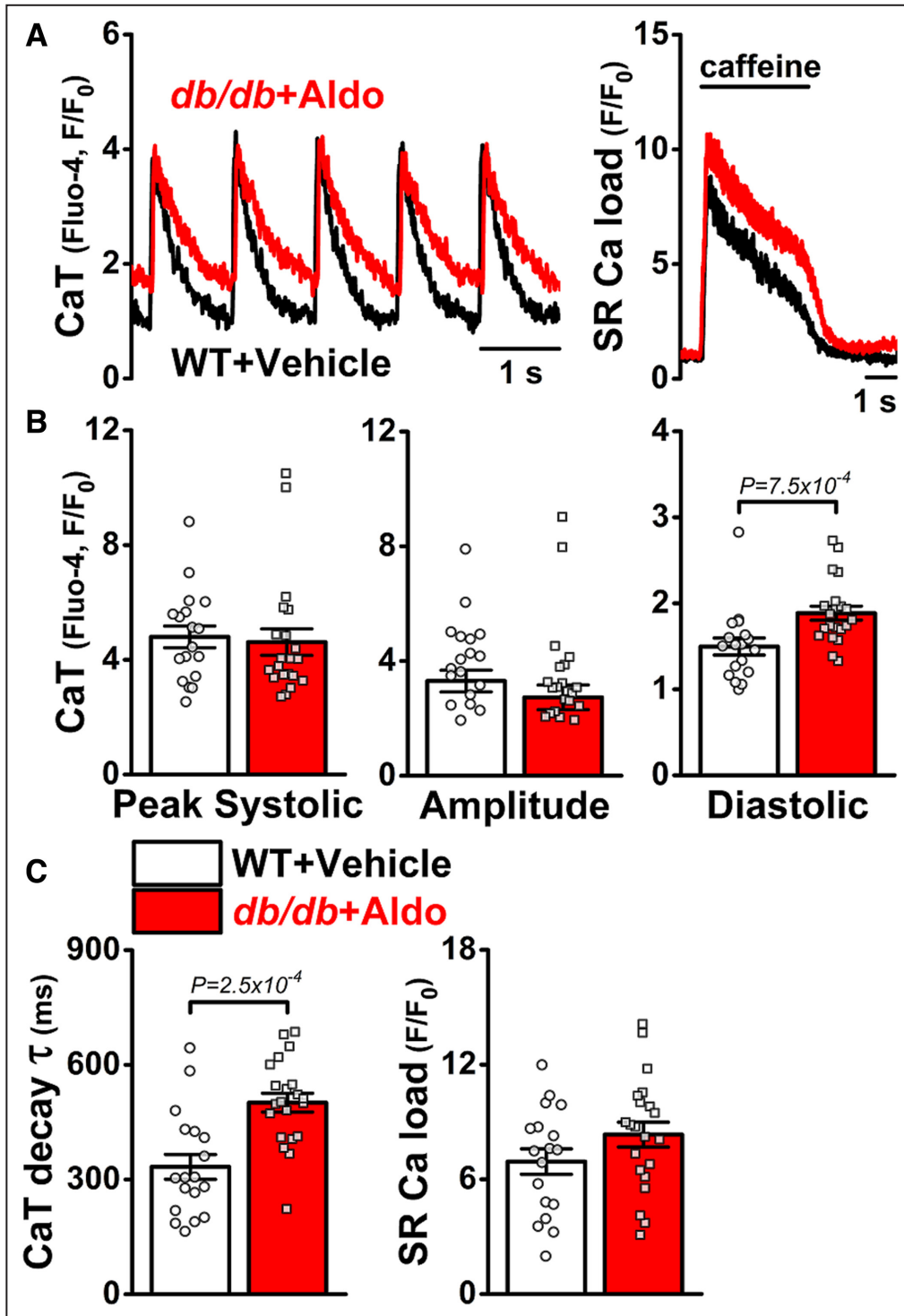


**Figure 4. Prolonged Ca transient decay in *db/db*+Aldo.**

**A**, Representative intracellular CaTs in WT+vehicle and *db/db*+Aldo cardiomyocytes at 1-Hz pacing and following a rapid caffeine pulse (10mmol/L). **B**, Intracellular Ca<sup>2+</sup> levels quantified as changes in Fluo-4 fluorescence. Diastolic [Ca<sup>2+</sup>]<sub>i</sub> is the ratio of minimum *F* between beats at 1Hz and the resting *F*<sub>0</sub>. **C**, Prolonged CaT decay tau and unchanged SR Ca<sup>2+</sup> content in *db/db*+Aldo. Mann-Whitney test. Mean±SEM is shown. n=18 cells from 6 animals in WT+vehicle and n=21 cells from 8 animals in *db/db*+Aldo. Each individual myocyte is shown as a data point. CaTs indicates Ca<sup>2+</sup> transients; *db/db*+Aldo, *db/db* mice with chronic aldosterone infusion; SR, sarcoplasmic reticulum; and WT, wild-type.

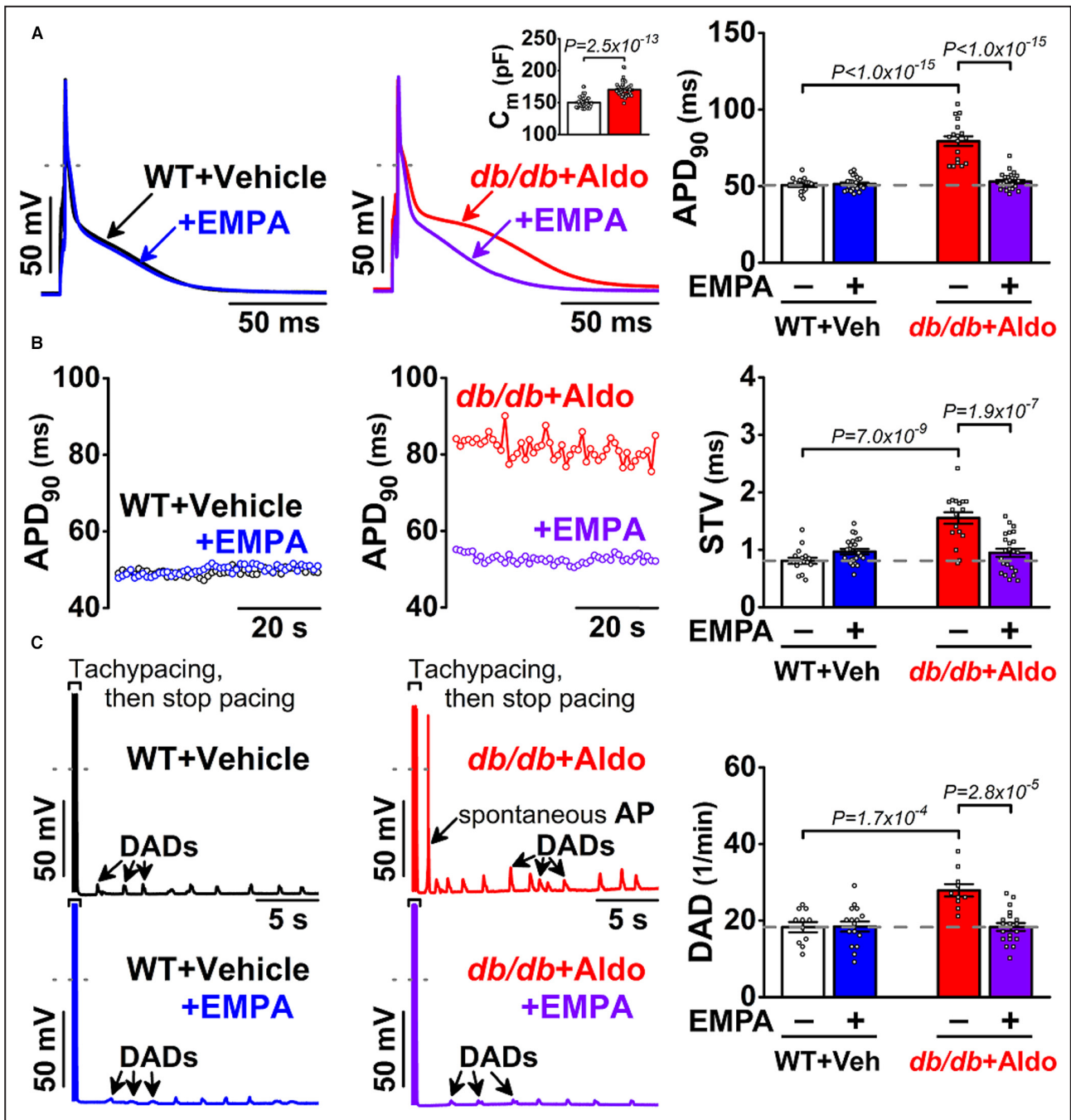


**Figure 5. Arrhythmogenic AP changes in *db/db*+Aldo murine cardiomyocytes are reversed by empagliflozin.** **A**, Representative APs in WT+vehicle and *db/db*+Aldo cardiomyocytes at 1-Hz pacing.  $C_m$  is shown in the inset (Mann–Whitney test). Prolongation of APD<sub>90</sub> in *db/db*+Aldo is reversed by EMPA (1  $\mu$ mol/L, 4 hours). **B**, STV of APD<sub>90</sub> was increased in *db/db*+Aldo, and this increase was reversed by EMPA. In AP measurements, 16 cells from 7 animals in WT+vehicle without EMPA treatment; 23 cells from 7 animals in WT+vehicle with EMPA treatment; 18 cells from 8 animals in *db/db*+Aldo without EMPA treatment; and 23 cells from 8 animals in *db/db*+Aldo with EMPA treatment. **C**, DADs and spontaneous APs were increased in *db/db*+Aldo following cessation of tachypacing (10 Hz) and reversed by EMPA. In DAD measurements, 11 cells from 7 animals in WT+vehicle without EMPA treatment; 16 cells from 7 animals in WT+vehicle with EMPA treatment; 10 cells from 8 animals in *db/db*+Aldo without EMPA treatment; and 19 cells from 8 animals in *db/db*+Aldo with EMPA treatment. Mean $\pm$ SEM is shown. ANOVA followed by Tukey multiple comparisons test. Each individual myocyte is shown as a data point. AP indicates action potential; APD<sub>90</sub>, AP duration at 90% repolarization;  $C_m$ , cell capacitance; DADs, delayed afterdepolarizations; *db/db*+Aldo, *db/db* mice with chronic aldosterone infusion; EMPA, empagliflozin pretreatment; STV, short-term variability; and WT, wild-type.

and spontaneous APs were significantly increased in *db/db*+Aldo mice (Figure 5C). Importantly, all proarrhythmic AP changes were reversed by empagliflozin pretreatment (1  $\mu\text{mol/L}$ , 4 hours) in *db/db*+Aldo mice, while empagliflozin had no effect in WT+vehicle control mice (Figure 5A through 5C).

### Late Na<sup>+</sup> Current Is Enhanced in *db/db*+Aldo Murine Cardiomyocytes

APD prolongation, predominantly at phase 3 repolarization (Figure 5; Figure S3), suggested a potential role for  $I_{\text{Na,Late}}$  enhancement in *db/db*+Aldo myocytes.  $I_{\text{Na,Late}}$  density (current amplitude normalized to cell

capacitance) was markedly increased in *db/db*+Aldo (Figure 6). Importantly, empagliflozin preincubation (1  $\mu\text{mol/L}$ , 4 hours) reversed  $I_{\text{Na,Late}}$  upregulation in *db/db*+Aldo mice and had no effects in controls (Figure 6), in line with the significant effect of empagliflozin selectively on APD in *db/db*+Aldo versus WT+vehicle (Figure 5).

## DISCUSSION

### Modeling Diabetic HFpEF in Preclinical Research

Diabetes and mineralocorticoid excess are associated with worse outcome in patients with HFpEF.<sup>6,22,33</sup>

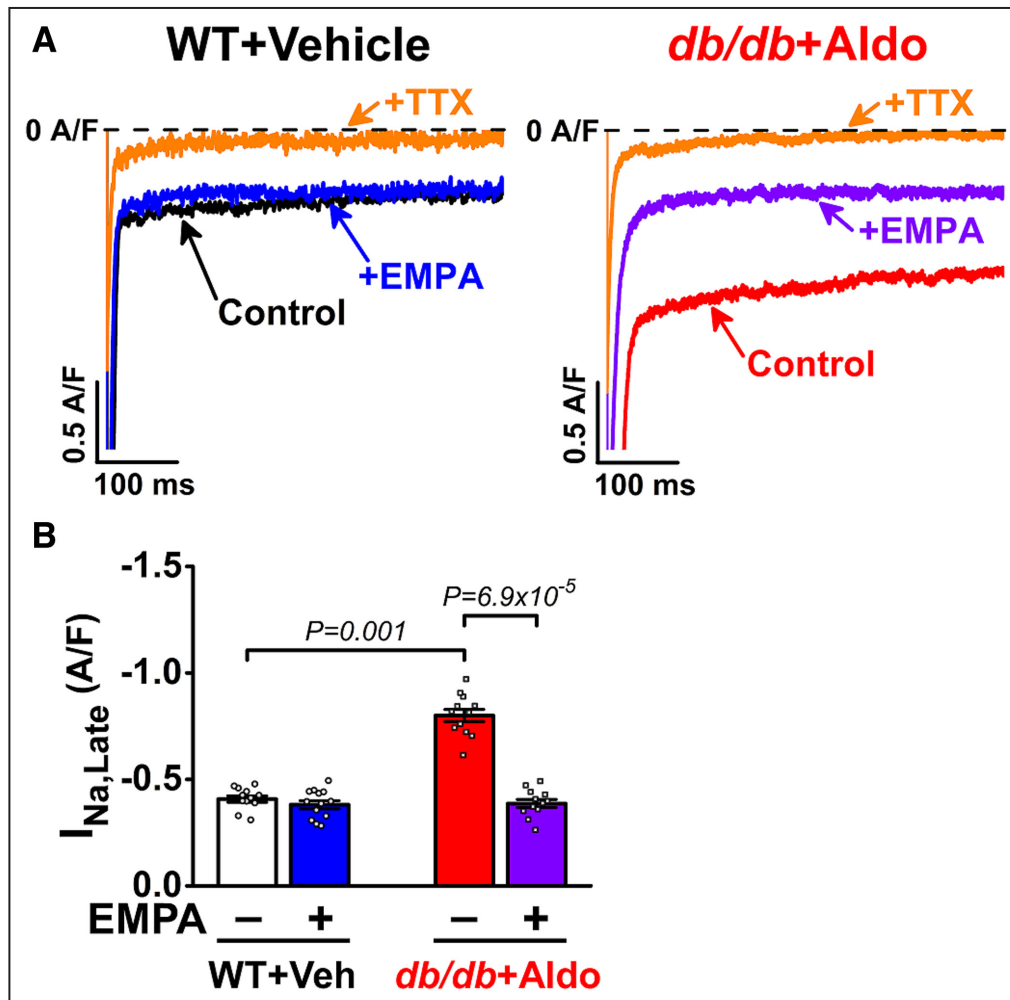


**Figure 6.** Empagliflozin reverses late Na<sup>+</sup> current enhancement in *db/db*+Aldo murine cardiomyocytes.

**A**, Representative  $I_{\text{Na,Late}}$  traces in WT+vehicle and *db/db*+Aldo myocytes without or with preincubation with EMPA (1  $\mu\text{mol/L}$ , 4 hours) and subsequent acute TTX (10  $\mu\text{mol/L}$ , 3 minutes) applications. (Peak  $I_{\text{Na}}$  was off-scale.) **B**, EMPA pretreatment reversed  $I_{\text{Na,Late}}$  upregulation in *db/db*+Aldo. Mean  $\pm$  SEM is shown. ANOVA followed by Dunn multiple comparisons test. 12 cells from 4 animals in WT+vehicle without EMPA treatment; 13 cells from 4 animals in WT+vehicle with EMPA treatment; 12 cells from 4 animals in *db/db*+Aldo without EMPA treatment; and 12 cells from 4 animals in *db/db*+Aldo with EMPA treatment. Each individual myocyte is shown as a data point. *db/db*+Aldo indicates *db/db* mice with chronic aldosterone infusion; EMPA, empagliflozin pretreatment;  $I_{\text{Na,Late}}$ , late Na<sup>+</sup> current; TTX, tetrodotoxin; and WT, wild-type.

In preclinical research, *db/db* and aldosterone infusion models have been used independently to study HFpEF disease mechanisms.<sup>19,21</sup> However, *db/db* mice or aldosterone-treated WT mice only exhibit a mild diastolic dysfunction (Figure 3), in line with previous reports, and fail to recapitulate the complex metabolic and hemodynamic derangements in HFpEF.<sup>10,11,18</sup> The cardiac systolic function tends to decrease with age in *db/db* mice<sup>34</sup>; however, the additional hemodynamic challenge caused by excess aldosterone led to preserved EF in *db/db*+Aldo mice (Figure 3). In line with this, *db/db* mice did not develop heart failure with reduced EF following pressure overload induced by transverse aortic constriction.<sup>35</sup> This was associated with restoration of protein kinase D1 function,<sup>35</sup> which importantly regulates cardiac hypertrophy and progression to heart failure with reduced EF.<sup>36</sup> Aldosterone infusion alone induces mild changes in cardiac function unless accompanied by additional stressors (eg, uninephrectomy+salt water<sup>21</sup> or myocardial infarction).<sup>37</sup> Here we showed that combined *db/db*+Aldo synergistically induces marked diastolic dysfunction, concentric cardiac hypertrophy, pulmonary congestion, and multiple common comorbidities of HFpEF, including diabetes, obesity, and increased vascular resistance (Figures 1 through 3), more closely recapitulating important aspects of human HFpEF. Thus, our new 2-hit HFpEF model (*db/db*+Aldo) complements other recent preclinical models with a somewhat different disease pathophysiology (eg, versus a model of nitrosative stress in high-fat diet+L-NAME-treated mice<sup>14</sup>). Indeed, individual HFpEF animal models (including this *db/db*+Aldo model) may best phenocopy a different subset of patients with HFpEF,<sup>12,22–24</sup> each of which may benefit most by different targeted therapeutic strategies. Parallel use of these translational HFpEF models can help to better understand disease pathomechanisms, find new molecular targets, test new drugs, and stratify subgroups of patients with HFpEF with prognostic and therapeutic implications.<sup>1,13</sup>

### Mechanisms of Increased Arrhythmia Susceptibility in Diabetic HFpEF

The *db/db*+Aldo model showed proarrhythmic changes in Ca<sup>2+</sup> handling (Figure 4) and electrophysiology (Figures 5 and 6), in line with the increased arrhythmia susceptibility in diabetic patients with HFpEF.<sup>6,22</sup> The QTc is longer in patients with HFpEF,<sup>2</sup> and an increased incidence of nonsustained ventricular tachycardia was reported on their ambulatory ECGs,<sup>2,3</sup> correlating with APD prolongation and increased delayed afterdepolarizations in *db/db*+Aldo mice (Figure 5). Diabetic hyperglycemia has been shown to induce a complex signaling network of oxidative stress,

intracellular glycosylation, and activation of protein kinases (Ca<sup>2+</sup>/calmodulin-dependent protein kinase II, protein kinase C, protein kinase D1), which impairs the function of multiple sarcolemmal and sarcoplasmic ion channels to promote proarrhythmic APs.<sup>26,38–40</sup> Noncardiomyocyte mechanisms, including inflammation, fibrosis, and coronary artery disease may further enhance arrhythmias in diabetic HFpEF.<sup>38</sup> We also show elevated arterial myogenic tone at physiological arterial pressures (Figure 2), which could contribute to hypertension observed in many patients with HFpEF. The increased mechanical afterload caused by hypertension can further enhance arrhythmogenic Ca<sup>2+</sup> handling and ion channel functional impairments in cardiac myocytes, dependent on nitric oxide signaling.<sup>41,42</sup>

### Potential Ionic Mechanisms and Antiarrhythmic Effects of Empagliflozin in HFpEF

Empagliflozin reduces mortality and hospitalization in patients with HFpEF with or without diabetes.<sup>8</sup> In line with this, SGLT2 inhibitors were shown to provide direct cardiovascular benefits beyond glycemic control.<sup>25,43</sup> Moreover, SGLT2 expression is lacking in cardiomyocytes,<sup>44</sup> suggesting an off-target effect. The sodium-hydrogen exchanger has been suggested as a potential empagliflozin target in cardiomyocytes<sup>45</sup>; however, this mechanism remains controversial.<sup>46</sup> Another target for SGLT2 inhibitors in cardiomyocytes can be the late Na<sup>+</sup> current.<sup>47</sup> Recently, we showed that empagliflozin reversed the enhancement of late Na<sup>+</sup> current and APD prolongation in a different HFpEF model induced by high-fat diet+L-NAME treatment.<sup>48</sup> However, this empagliflozin effect on late Na<sup>+</sup> current and APD in HFpEF required drug preincubation for 4 hours and suggested that the effect could be mediated by reduction of oxidative stress and suppression of Ca<sup>2+</sup>/calmodulin-dependent protein kinase II.<sup>48,49</sup> Here we confirm this therapeutic benefit of empagliflozin in an additional HFpEF model, showing a complete reversal of  $I_{Na,Late}$  enhancement and proarrhythmic AP changes in *db/db*+Aldo cardiomyocytes (Figures 5 and 6). Thus, empagliflozin might have beneficial electrophysiological effects by reversing the cellular Na<sup>+</sup> and Ca<sup>2+</sup>-handling impairments, which form a vicious cycle promoting contractile dysfunction and arrhythmias in the failing heart.<sup>31</sup> While the potential antiarrhythmic effects of SGLT2 inhibitors in patients with HFpEF are yet to be determined, dapagliflozin reduced the risk of ventricular arrhythmias and sudden cardiac death in patients with heart failure with reduced EF.<sup>50</sup> Dapagliflozin also attenuated diastolic dysfunction in a similar mouse model presented here, which used chronic angiotensin II infusion in *db/db* mice.<sup>51</sup>

## Study Limitations

Aging, an important characteristic of patients with HFpEF, has not been considered in this animal model.<sup>11</sup> In addition to arrhythmogenic ventricular remodeling, atrial fibrillation is a frequent comorbidity in aging patients with HFpEF,<sup>52,53</sup> which requires further investigation. Sex differences and the underlying molecular mechanisms were not studied here; however, cardiac remodeling is more prominent in diabetic women with HFpEF,<sup>54</sup> and female *db/db* mice,<sup>20</sup> and mineralocorticoid receptor inhibition may provide more benefit in women with HFpEF.<sup>55</sup>

## CONCLUSIONS

In the current study, we showed that diabetes and excess aldosterone synergistically promote diastolic dysfunction, concentric cardiac hypertrophy, elevated BNP levels, and significant extracardiac comorbidities (including severe obesity, diabetes with marked hyperglycemia, pulmonary edema, and vascular dysfunction), recapitulating important aspects of human HFpEF. At the level of cardiac myocytes, diabetes and excess aldosterone induced diastolic Ca<sup>2+</sup>-handling impairments and APD prolongation and enhanced *I*<sub>Na,Late</sub>, which could promote diastolic dysfunction and arrhythmias in this murine model of HFpEF. Empagliflozin reversed *I*<sub>Na,Late</sub> enhancement and cellular proarrhythmia, directly acting on murine HFpEF myocytes. In conclusion, the *db/db*+Aldo model represents an important clinical subgroup of HFpEF that has marked hyperglycemia and obesity and increased arrhythmia risk. This novel HFpEF model can be useful to better understand disease pathobiology and therapeutic effects.

## ARTICLE INFORMATION

Received June 15, 2022; accepted October 25, 2022.

### Affiliations

Department of Pharmacology, University of California, Davis, CA (B.H., J.M.H., C.Y.K., J.H., E.Y.S., E.R.S., D.S., M.F.N., D.M.B., J.B.); and Research Group in Veterinary Medicine (GIVET), School of Veterinary Medicine, University Corporation Lasallista (Unilasallista), Caldas, Antioquia, Colombia (J.M.H.).

### Acknowledgments

We thank Mukul Sharda, Adam Wilder, Anastasia Krajinovic, Vicky Diep, and Megan Ngim for their help in animal care, tissue collection, and laboratory tasks.

### Sources of Funding

This work was supported by grants from the National Institutes of Health: P01-HL141084 (Bers), R01-HL142282 (Bers and Bossuyt), and R01-HL149127 (Navedo); and the Minciencias – Fulbright Colombia (Mira Hernandez).

### Disclosures

None.

### Supplemental Material

Data S1  
Figures S1–S3

## REFERENCES

- Shah SJ, Borlaug BA, Kitzman DW, McCulloch AD, Blaxall BC, Agarwal R, Chirinos JA, Collins S, Deo RC, Gladwin MT, et al. Research priorities for heart failure with preserved ejection fraction: National Heart, Lung, and Blood Institute working group summary. *Circulation*. 2020;141:1001–1026. doi: [10.1161/CIRCULATIONAHA.119.041886](https://doi.org/10.1161/CIRCULATIONAHA.119.041886)
- Cho JH, Leong D, Cuk N, Ebinger JE, Bresee C, Yoon SH, Ehdai A, Shehata M, Wang X, Chugh SS, et al. Delayed repolarization and ventricular tachycardia in patients with heart failure and preserved ejection fraction. *PLoS One*. 2021;16:e0254641. doi: [10.1371/journal.pone.0254641](https://doi.org/10.1371/journal.pone.0254641)
- Gutierrez A, Ash J, Akdemir B, Alexy T, Cogswell R, Chen J, Adabag S. Nonsustained ventricular tachycardia in heart failure with preserved ejection fraction. *Pacing Clin Electrophysiol*. 2020;43:1126–1131. doi: [10.1111/pace.14043](https://doi.org/10.1111/pace.14043)
- Chan MM, Lam CS. How do patients with heart failure with preserved ejection fraction die? *Eur J Heart Fail*. 2013;15:604–613. doi: [10.1093/eurjhf/hft062](https://doi.org/10.1093/eurjhf/hft062)
- Tromp J, MacDonald MR, Tay WT, Teng TK, Hung CL, Narasimhan C, Shimizu W, Ling LH, Ng TP, Yap J, et al. Heart failure with preserved ejection fraction in the young. *Circulation*. 2018;138:2763–2773. doi: [10.1161/CIRCULATIONAHA.118.034720](https://doi.org/10.1161/CIRCULATIONAHA.118.034720)
- Vaduganathan M, Claggett BL, Chatterjee NA, Anand IS, Sweitzer NK, Fang JC, O'Meara E, Shah SJ, Hegde SM, Desai AS, et al. Sudden death in heart failure with preserved ejection fraction: a competing risks analysis from the TOPCAT trial. *JACC Heart Fail*. 2018;6:653–661. doi: [10.1016/j.jchf.2018.02.014](https://doi.org/10.1016/j.jchf.2018.02.014)
- Pfeffer MA, Claggett B, Assmann SF, Boineau R, Anand IS, Clausell N, Desai AS, Diaz R, Fleg JL, Gordeev I, et al. Regional variation in patients and outcomes in the treatment of preserved cardiac function heart failure with an aldosterone antagonist (TOPCAT) trial. *Circulation*. 2015;131:34–42. doi: [10.1161/CIRCULATIONAHA.114.013255](https://doi.org/10.1161/CIRCULATIONAHA.114.013255)
- Anker SD, Butler J, Filippatos G, Ferreira JP, Bocchi E, Bohm M, Brunner-La Rocca HP, Choi DJ, Chopra V, Chuquiere-Valenzuela E, et al. Empagliflozin in heart failure with a preserved ejection fraction. *N Engl J Med*. 2021;385:1451–1461. doi: [10.1056/NEJMoa2107038](https://doi.org/10.1056/NEJMoa2107038)
- Solomon SD, McMurray JJV, Claggett B, de Boer RA, DeMetts D, Hernandez AF, Inzucchi SE, Kosiborod MN, Lam CSP, Martinez F, et al. Dapagliflozin in heart failure with mildly reduced or preserved ejection fraction. *N Engl J Med*. 2022;387:1089–1098. doi: [10.1056/NEJMoa2206286](https://doi.org/10.1056/NEJMoa2206286)
- Mishra S, Kass DA. Cellular and molecular pathobiology of heart failure with preserved ejection fraction. *Nat Rev Cardiol*. 2021;18:400–423. doi: [10.1038/s41569-020-00480-6](https://doi.org/10.1038/s41569-020-00480-6)
- Withaar C, Lam CSP, Schiattarella GG, de Boer RA, Meems LMG. Heart failure with preserved ejection fraction in humans and mice: embracing clinical complexity in mouse models. *Eur Heart J*. 2021;42:4420–4430. doi: [10.1093/eurheartj/ehab389](https://doi.org/10.1093/eurheartj/ehab389)
- Roh J, Hill JA, Singh A, Valero-Munoz M, Sam F. Heart failure with preserved ejection fraction: heterogeneous syndrome, diverse preclinical models. *Circ Res*. 2022;130:1906–1925. doi: [10.1161/CIRCRESAHA.122.320257](https://doi.org/10.1161/CIRCRESAHA.122.320257)
- Smith AN, Altara R, Amin G, Habeichi NJ, Thomas DG, Jun S, Kaplan A, Booz GW, Zouein FA. Genomic, proteomic, and metabolic comparisons of small animal models of heart failure with preserved ejection fraction: a tale of mice, rats, and cats. *J Am Heart Assoc*. 2022;11:e026071. doi: [10.1161/JAHA.122.026071](https://doi.org/10.1161/JAHA.122.026071)
- Schiattarella GG, Altamirano F, Tong D, French KM, Villalobos E, Kim SY, Luo X, Jiang N, May HI, Wang ZV, et al. Nitrosative stress drives heart failure with preserved ejection fraction. *Nature*. 2019;568:351–356. doi: [10.1038/s41586-019-1100-z](https://doi.org/10.1038/s41586-019-1100-z)
- Lai YC, Tabima DM, Dube JJ, Hughan KS, Vanderpool RR, Goncharov DA, St Croix CM, Garcia-Ocana A, Goncharova EA, Tofovic SP, et al. SIRT3-AMP-activated protein kinase activation by nitrite and metformin improves hyperglycemia and normalizes pulmonary hypertension associated with heart failure with preserved ejection fraction. *Circulation*. 2016;133:717–731. doi: [10.1161/CIRCULATIONAHA.115.018935](https://doi.org/10.1161/CIRCULATIONAHA.115.018935)
- Olver TD, Edwards JC, Jurrissen TJ, Veteto AB, Jones JL, Gao C, Rau C, Warren CM, Klutho PJ, Alex L, et al. Western diet-fed, aortic-banded Ossabaw swine: a preclinical model of cardio-metabolic heart failure. *JACC Basic Transl Sci*. 2019;4:404–421. doi: [10.1016/j.jacbts.2019.02.004](https://doi.org/10.1016/j.jacbts.2019.02.004)
- Sharp TE III, Scarborough AL, Li Z, Polhemus DJ, Hidalgo HA, Schumacher JD, Matsuura TR, Jenkins JS, Kelly DP, Goodchild TT,

- et al. Novel Gottingen Miniswine model of heart failure with preserved ejection fraction integrating multiple comorbidities. *JACC Basic Transl Sci.* 2021;6:154–170. doi: [10.1016/j.jacbts.2020.11.012](https://doi.org/10.1016/j.jacbts.2020.11.012)
18. Valero-Munoz M, Backman W, Sam F. Murine models of heart failure with preserved ejection fraction: a "fishing expedition.". *JACC Basic Transl Sci.* 2017;2:770–789. doi: [10.1016/j.jacbts.2017.07.013](https://doi.org/10.1016/j.jacbts.2017.07.013)
  19. Belke DD, Larsen TS, Gibbs EM, Severson DL. Altered metabolism causes cardiac dysfunction in perfused hearts from diabetic (db/db) mice. *Am J Physiol Endocrinol Metab.* 2000;279:E1104–E1113. doi: [10.1152/ajpendo.2000.279.5.E1104](https://doi.org/10.1152/ajpendo.2000.279.5.E1104)
  20. Alex L, Russo I, Holoborodko V, Frangogiannis NG. Characterization of a mouse model of obesity-related fibrotic cardiomyopathy that recapitulates features of human heart failure with preserved ejection fraction. *Am J Physiol Heart Circ Physiol.* 2018;315:H934–H949. doi: [10.1152/ajpheart.00238.2018](https://doi.org/10.1152/ajpheart.00238.2018)
  21. Valero-Munoz M, Li S, Wilson RM, Boldbaatar B, Iglarz M, Sam F. Dual endothelin-a/endothelin-B receptor blockade and cardiac remodeling in heart failure with preserved ejection fraction. *Circ Heart Fail.* 2016;9:9. doi: [10.1161/CIRCHEARTFAILURE.116.003381](https://doi.org/10.1161/CIRCHEARTFAILURE.116.003381)
  22. Cohen JB, Schrauben SJ, Zhao L, Basso MD, Cvijic ME, Li Z, Yarde M, Wang Z, Bhattacharya PT, Chirinos DA, et al. Clinical phenogroups in heart failure with preserved ejection fraction: detailed phenotypes, prognosis, and response to spironolactone. *JACC Heart Fail.* 2020;8:172–184. doi: [10.1016/j.jchf.2019.09.009](https://doi.org/10.1016/j.jchf.2019.09.009)
  23. Hahn VS, Knutsdottir H, Luo X, Bedi K, Margulies KB, Haldar SM, Stolina M, Yin J, Khakoo AY, Vaishnav J, et al. Myocardial gene expression signatures in human heart failure with preserved ejection fraction. *Circulation.* 2021;143:120–134. doi: [10.1161/CIRCULATIONNAHA.120.050498](https://doi.org/10.1161/CIRCULATIONNAHA.120.050498)
  24. Frisk M, Le C, Shen X, Roe AT, Hou Y, Manfra O, Silva GJJ, van Hout I, Norden ES, Aronsen JM, et al. Etiology-dependent impairment of diastolic cardiomyocyte calcium homeostasis in heart failure with preserved ejection fraction. *J Am Coll Cardiol.* 2021;77:405–419. doi: [10.1016/j.jacc.2020.11.044](https://doi.org/10.1016/j.jacc.2020.11.044)
  25. Cowie MR, Fisher M. SGLT2 inhibitors: mechanisms of cardiovascular benefit beyond glycaemic control. *Nat Rev Cardiol.* 2020;17:761–772. doi: [10.1038/s41569-020-0406-8](https://doi.org/10.1038/s41569-020-0406-8)
  26. Hegyi B, Fasoli A, Ko CY, Van BW, Alim CC, Shen EY, Ciccozzi MM, Tapa S, Ripplinger CM, Erickson JR, et al. CaMKII serine 280 O-GlcNAcylation links diabetic hyperglycemia to proarrhythmia. *Circ Res.* 2021;129:98–113. doi: [10.1161/CIRCRESAHA.120.318402](https://doi.org/10.1161/CIRCRESAHA.120.318402)
  27. Le T, Martin-Aragon Baudel M, Syed A, Singhrao N, Pan S, Flores-Tamez VA, Burns AE, Man KNM, Karey E, Hong J, et al. Secondhand smoke exposure impairs ion channel function and contractility of mesenteric arteries. *Function (Oxf).* 2021;2:zqab041. doi: [10.1093/function/zqab041](https://doi.org/10.1093/function/zqab041)
  28. Tsang TS, Barnes ME, Gersh BJ, Bailey KR, Seward JB. Left atrial volume as a morphophysiological expression of left ventricular diastolic dysfunction and relation to cardiovascular risk burden. *Am J Cardiol.* 2002;90:1284–1289. doi: [10.1016/s0002-9149\(02\)02864-3](https://doi.org/10.1016/s0002-9149(02)02864-3)
  29. Zile MR, Gottdiener JS, Hetzel SJ, McMurray JJ, Komajda M, McKelvie R, Baicu CF, Massie BM, Carson PE, Investigators IP. Prevalence and significance of alterations in cardiac structure and function in patients with heart failure and a preserved ejection fraction. *Circulation.* 2011;124:2491–2501. doi: [10.1161/CIRCULATIONNAHA.110.011031](https://doi.org/10.1161/CIRCULATIONNAHA.110.011031)
  30. Bers DM. Cardiac excitation-contraction coupling. *Nature.* 2002;415:198–205. doi: [10.1038/415198a](https://doi.org/10.1038/415198a)
  31. Hegyi B, Polonen RP, Hellgren KT, Ko CY, Ginsburg KS, Bossuyt J, Mercola M, Bers DM. Cardiomyocyte Na<sup>+</sup> and Ca<sup>2+</sup> mishandling drives vicious cycle involving CaMKII, ROS, and ryanodine receptors. *Basic Res Cardiol.* 2021;116:58. doi: [10.1007/s00395-021-00900-9](https://doi.org/10.1007/s00395-021-00900-9)
  32. Johnson DM, Heijman J, Bode EF, Greensmith DJ, van der Linde H, Abi-Gerges N, Eisner DA, Trafford AW, Volders PG. Diastolic spontaneous calcium release from the sarcoplasmic reticulum increases beat-to-beat variability of repolarization in canine ventricular myocytes after beta-adrenergic stimulation. *Circ Res.* 2013;112:246–256. doi: [10.1161/CIRCRESAHA.112.275735](https://doi.org/10.1161/CIRCRESAHA.112.275735)
  33. Lindman BR, Davila-Roman VG, Mann DL, McNulty S, Semigran MJ, Lewis GD, de las Fuentes L, Joseph SM, Vader J, Hernandez AF, et al. Cardiovascular phenotype in HFpEF patients with or without diabetes: a RELAX trial ancillary study. *J Am Coll Cardiol.* 2014;64:541–549. doi: [10.1016/j.jacc.2014.05.030](https://doi.org/10.1016/j.jacc.2014.05.030)
  34. Aasum E, Hafstad AD, Severson DL, Larsen TS. Age-dependent changes in metabolism, contractile function, and ischemic sensitivity in hearts from db/db mice. *Diabetes.* 2003;52:434–441. doi: [10.2337/diabetes.52.2.434](https://doi.org/10.2337/diabetes.52.2.434)
  35. Abdurrachim D, Nabben M, Hoerr V, Kuhlmann MT, Bovenkamp P, Ciapaitis J, Geraets IME, Coumans W, Luiken J, Glatz JF, et al. Diabetic db/db mice do not develop heart failure upon pressure overload: a longitudinal in vivo PET, MRI, and MRS study on cardiac metabolic, structural, and functional adaptations. *Cardiovasc Res.* 2017;113:1148–1160. doi: [10.1093/cvr/cvx100](https://doi.org/10.1093/cvr/cvx100)
  36. Bossuyt J, Borst JM, Verberckmoes M, Bailey LR, Bers DM, Hegyi B. Protein kinase D1 regulates cardiac hypertrophy, potassium channel remodeling, and arrhythmias in heart failure. *J Am Heart Assoc.* 2022;11:e027573. doi: [10.1161/JAHA.122.027573](https://doi.org/10.1161/JAHA.122.027573)
  37. He BJ, Joiner ML, Singh MV, Luczak ED, Swaminathan PD, Koval OM, Kutschke W, Allamargot C, Yang J, Guan X, et al. Oxidation of CaMKII determines the cardiotoxic effects of aldosterone. *Nat Med.* 2011;17:1610–1618. doi: [10.1038/nm.2506](https://doi.org/10.1038/nm.2506)
  38. Hegyi B, Bers DM, Bossuyt J. CaMKII signaling in heart diseases: emerging role in diabetic cardiomyopathy. *J Mol Cell Cardiol.* 2019;127:246–259. doi: [10.1016/j.yjmcc.2019.01.001](https://doi.org/10.1016/j.yjmcc.2019.01.001)
  39. Hegyi B, Borst JM, Bailey LRJ, Shen EY, Lucena AJ, Navedo MF, Bossuyt J, Bers DM. Hyperglycemia regulates cardiac K<sup>+</sup> channels via O-GlcNAc-CaMKII and NOX2-ROS-PKC pathways. *Basic Res Cardiol.* 2020;115:71. doi: [10.1007/s00395-020-00834-8](https://doi.org/10.1007/s00395-020-00834-8)
  40. Hegyi B, Ko CY, Bossuyt J, Bers DM. Two-hit mechanism of cardiac arrhythmias in diabetic hyperglycaemia: reduced repolarization reserve, neurohormonal stimulation, and heart failure exacerbate susceptibility. *Cardiovasc Res.* 2021;117:2781–2793. doi: [10.1093/cvr/cvab006](https://doi.org/10.1093/cvr/cvab006)
  41. Shimkunas R, Hegyi B, Jian Z, Shaw JA, Kazemi-Lari MA, Mitra D, Leach JK, Li X, Jaradeh M, Balardi N, et al. Mechanical load regulates excitation-Ca<sup>2+</sup> signaling-contraction in cardiomyocyte. *Circ Res.* 2021;128:772–774. doi: [10.1161/CIRCRESAHA.120.318570](https://doi.org/10.1161/CIRCRESAHA.120.318570)
  42. Hegyi B, Shimkunas R, Jian Z, Izu LT, Bers DM, Chen-Izu Y. Mechanoelectric coupling and arrhythmogenesis in cardiomyocytes contracting under mechanical afterload in a 3D viscoelastic hydrogel. *Proc Natl Acad Sci USA.* 2021;118:118. doi: [10.1073/pnas.2108484118](https://doi.org/10.1073/pnas.2108484118)
  43. Lopaschuk GD, Verma S. Mechanisms of cardiovascular benefits of sodium glucose Co-transporter 2 (SGLT2) inhibitors: a state-of-the-art review. *JACC Basic Transl Sci.* 2020;5:632–644. doi: [10.1016/j.jacbts.2020.02.004](https://doi.org/10.1016/j.jacbts.2020.02.004)
  44. von Lewinski D, Rainer PP, Gasser R, Huber MS, Khafaga M, Wilhelm B, Haas T, Machler H, Rossli U, Pieske B. Glucose-transporter-mediated positive inotropic effects in human myocardium of diabetic and nondiabetic patients. *Metabolism.* 2010;59:1020–1028. doi: [10.1016/j.metabol.2009.10.025](https://doi.org/10.1016/j.metabol.2009.10.025)
  45. Baartscheer A, Schumacher CA, Wust RC, Fiolet JW, Stienen GJ, Coronel R, Zuurbier CJ. Empagliflozin decreases myocardial cytoplasmic Na<sup>(+)</sup> through inhibition of the cardiac Na<sup>(+)</sup>/H<sup>(+)</sup> exchanger in rats and rabbits. *Diabetologia.* 2017;60:568–573. doi: [10.1007/s00125-016-4134-x](https://doi.org/10.1007/s00125-016-4134-x)
  46. Chung YJ, Park KC, Tokar S, Eykyn TR, Fuller W, Pavlovic D, Swietach P, Shattock MJ. Off-target effects of sodium-glucose co-transporter 2 blockers: empagliflozin does not inhibit Na<sup>+</sup>/H<sup>+</sup> exchanger-1 or lower [Na<sup>+</sup>]<sub>i</sub> in the heart. *Cardiovasc Res.* 2021;117:2794–2806. doi: [10.1093/cvr/cvaa323](https://doi.org/10.1093/cvr/cvaa323)
  47. Philippaert K, Kalyaanamoorthy S, Fatehi M, Long W, Soni S, Byrne NJ, Barr A, Singh J, Wong J, Palechuk T, et al. Cardiac late sodium channel current is a molecular target for the sodium/glucose cotransporter 2 inhibitor empagliflozin. *Circulation.* 2021;143:2188–2204. doi: [10.1161/CIRCULATIONNAHA.121.053350](https://doi.org/10.1161/CIRCULATIONNAHA.121.053350)
  48. Hegyi B, Mira Hernandez J, Shen EY, Habibi NR, Bossuyt J, Bers DM. Empagliflozin reverses late Na<sup>+</sup> current enhancement and cardiomyocyte proarrhythmia in a translational murine model of heart failure with preserved ejection fraction. *Circulation.* 2022;145:1029–1031. doi: [10.1161/CIRCULATIONNAHA.121.057237](https://doi.org/10.1161/CIRCULATIONNAHA.121.057237)
  49. Mustrup J, Wagemann O, Lucht CM, Trum M, Hammer KP, Sag CM, Lebek S, Tarnowski D, Reinders J, Perbellini F, et al. Empagliflozin reduces Ca/calmodulin-dependent kinase II activity in isolated ventricular cardiomyocytes. *ESC Heart Fail.* 2018;5:642–648. doi: [10.1002/ehf2.12336](https://doi.org/10.1002/ehf2.12336)
  50. Curtain JP, Docherty KF, Jhund PS, Petrie MC, Inzucchi SE, Kober L, Kosiborod MN, Martinez FA, Ponikowski P, Sabatine MS, et al. Effect of dapagliflozin on ventricular arrhythmias, resuscitated cardiac arrest, or sudden death in DAPA-HF. *Eur Heart J.* 2021;42:3727–3738. doi: [10.1093/eurheartj/ehab560](https://doi.org/10.1093/eurheartj/ehab560)

- 
51. Arow M, Waldman M, Yadin D, Nudelman V, Shainberg A, Abraham NG, Freimark D, Kornowski R, Aravot D, Hochhauser E, et al. Sodium-glucose cotransporter 2 inhibitor dapagliflozin attenuates diabetic cardiomyopathy. *Cardiovasc Diabetol*. 2020;19:7. doi: [10.1186/s12933-019-0980-4](https://doi.org/10.1186/s12933-019-0980-4)
  52. Packer M, Lam CSP, Lund LH, Redfield MM. Interdependence of atrial fibrillation and heart failure with a preserved ejection fraction reflects a common underlying atrial and ventricular myopathy. *Circulation*. 2020;141:4–6. doi: [10.1161/CIRCULATIONAHA.119.042996](https://doi.org/10.1161/CIRCULATIONAHA.119.042996)
  53. Hohendanner F, Bode D, Primessnig U, Guthof T, Doerr R, Jeuthe S, Reimers S, Zhang K, Bach D, Wakula P, et al. Cellular mechanisms of metabolic syndrome-related atrial decompensation in a rat model of HFpEF. *J Mol Cell Cardiol*. 2018;115:10–19. doi: [10.1016/j.yjmcc.2017.12.012](https://doi.org/10.1016/j.yjmcc.2017.12.012)
  54. Shi K, Yang MX, Huang S, Yan WF, Qian WL, Li Y, Guo YK, Yang ZG. Effect of diabetes mellitus on the development of left ventricular contractile dysfunction in women with heart failure and preserved ejection fraction. *Cardiovasc Diabetol*. 2021;20:185. doi: [10.1186/s12933-021-01379-3](https://doi.org/10.1186/s12933-021-01379-3)
  55. Merrill M, Sweitzer NK, Lindenfeld J, Kao DP. Sex differences in outcomes and responses to spironolactone in heart failure with preserved ejection fraction: a secondary analysis of TOPCAT trial. *JACC Heart Fail*. 2019;7:228–238. doi: [10.1016/j.jchf.2019.01.003](https://doi.org/10.1016/j.jchf.2019.01.003)

## **SUPPLEMENTAL MATERIAL**

## Data S1. SUPPLEMENTAL METHODS

### Implantation of osmotic minipumps

The osmotic minipumps (Alzet, model 2004) were prepared per manufacturer's instructions. Animals were anesthetized by isoflurane (1-5%) during the entire surgical procedure. Once the animal was anesthetized, fur on the back was removed with a depilatory. The operating field was disinfected with chlorhexidine solution and 70% ethanol. A 1.5 cm mid-scapular incision was made across the back perpendicular to the spine. A hemostatic clamp was inserted into the incision, and the subcutaneous tissue was spread by opening and closing the jaws of the hemostat to create a pocket for the pump. A pump filled with 200  $\mu$ L solution was inserted into the pocket, starting with the delivery portal. The wound was closed with pharmaceutical grade surgical glue. Additionally, for any incisions greater than 1.5 cm or when glue did not provide sufficient closure, 3 single non-continuous sutures were placed, and removed 7-10 days later. Recovery of animals was carefully monitored, and if the mice showed pain or distress upon regaining consciousness, a dose of analgesic (buprenorphine, 0.05-0.1 mg/kg, SC) was given immediately, and additional doses were given if pain and distress persisted upon re-evaluation every 12 hr over a 48 hr period. The pumps stayed in the mice for 4 weeks and continuously delivered *d*-aldosterone at a rate of 0.3  $\mu$ g/hour.

### Aldosterone and BNP measurements

Aldosterone and B-type natriuretic peptide (BNP) levels were measured from blood plasma using enzyme-linked immunosorbent assay (ELISA) kits specific to aldosterone (Cayman Chemical, Aldosterone ELISA kit, Item No. 501090) and mouse BNP (RayBiotech, EIAM-BNP-1) according to the manufacturers' instructions. Plasma was prepared from anticoagulated (EDTA) blood by centrifugation at 3220 g for 1 hour at 4°C. The protein concentrations were calculated using a standard curve generated with recombinant standards provided by the manufacturers. Three technical replicates were performed for each biological sample.

### Pressure myography

Freshly isolated third and fourth order mesenteric arteries (average diameter 150-180  $\mu$ m and 0.5-1 mm in length) were cannulated onto glass micropipettes and mounted on a 5 mL myograph chamber (Living System Instrumentation, St Albans, VT, USA). Arteries were equilibrated at 20 mmHg for an hour with a pressure servo controller pump (Living System Instrumentation). Vessels were perfused continuously with a physiological saline solution (PSS) containing (in mmol/L): 119 NaCl, 4.7 KCl, 1.2 KH<sub>2</sub>PO<sub>4</sub>, 1.2 MgCl<sub>2</sub>, 2 CaCl<sub>2</sub>, 7 glucose, 24 NaHCO<sub>3</sub> at 37° C. The PSS solution was bubbled with 95% O<sub>2</sub> and 5% CO<sub>2</sub> to maintain the pH at 7.4. Changes in internal diameter were continuously recorded at 10 frames/second and analyzed using the IonOptix edge detection software (IonOptix 6.6, Westwood, MA, USA). Arterial viability was tested by treatment with 60 mmol/L KCl solution and subsequent development of myogenic tone upon increasing intravascular pressure. Arteries that did not constrict robustly to the high KCl solution and further developed stable tone at 80 mmHg were discarded. Once the arteries had achieved stable myogenic tone, they were tested over a range of intravascular pressures (10 to 100 mmHg) to obtain the active diameter (DA). At the end of the experiment, the passive diameter (DP) was acquired over the same pressure range in a Ca<sup>2+</sup> free PSS ([mmol/L], 119 NaCl, 4.7 KCl, 1.2 KH<sub>2</sub>PO<sub>4</sub>, 1.2 MgCl<sub>2</sub>, 7 glucose, 24 NaHCO<sub>3</sub>, 5 EGTA) + 1  $\mu$ mol/L nifedipine to determine the maximal dilation. The percentage of myogenic tone was calculated as [(DP-DA)/DP]×100.

### Murine echocardiography

Systolic and diastolic ventricular heart functions of mice were assessed by transthoracic echocardiography using the Vevo 2100 echocardiography system (FUJIFILM VisualSonics, Toronto, ON, Canada) equipped with a 40 MHz linear probe. Mice fur was removed by a depilatory the day before echocardiography recordings. During recordings, mice were anesthetized with isoflurane inhalation (1.5%), which was later individually adjusted (between 1 to 3%) to achieve a stable heart rate between 350 to 450 beats/min to assess diastolic dysfunction (to avoid fusion of the waves) and 450 to 600 beats/min to assess systolic

cardiac function (to avoid depressed contractile function) in each animal. ECG monitoring was obtained using limb electrodes, and core temperature was carefully monitored and maintained at 37°C during the entire procedure. Left ventricular (LV) M-mode echocardiography in parasternal short-axis view was performed for assessment of LV dimensions and systolic function. Pulsed wave Doppler and tissue Doppler images were acquired to assess diastolic function. At least three consecutive cardiac cycles were sampled for each measurement taken, and blinded analysis was performed off-line.

### **Enzymatic isolation of ventricular cardiomyocytes**

Mice injected with heparin (400 U/kg body weight) and anesthetized with isoflurane (5% in an induction chamber, then 1.5-3% via nose cone). Hearts were excised and retrograde perfused on constant flow Langendorff apparatus (4 min, 37°C) with Ca<sup>2+</sup>-free normal Tyrode's solution, gassed with 100% O<sub>2</sub>. Then, the heart was perfused for 13-16 min with 80 mg collagenase (type 2, Worthington Biochemical Corp., Lakewood, NJ, USA) and 1.4 mg protease (type XIV, Sigma-Aldrich, St. Louis, MO, USA) in 50 mL Tyrode's solution (with 10 µmol/L Ca<sup>2+</sup>) to enzymatically isolate cardiomyocytes. Following digestion, the myocytes were gently triturated with a pipette, then filtered through a nylon mesh and allowed to sediment for ~10 min. The sedimentation was repeated three times using increasing [Ca<sup>2+</sup>] from 0.125 to 0.25 then 0.5 mmol/L. Finally, ventricular myocytes were kept in Tyrode's solution (0.5 mmol/L Ca<sup>2+</sup>) at room temperature until use.

### **Calcium imaging**

Intracellular Ca<sup>2+</sup> transients and diastolic Ca<sup>2+</sup> events (sparks and waves) were measured in freshly isolated ventricular cardiomyocytes loaded with Fluo-4 AM (10 µmol/L, Invitrogen, Waltham, MA, USA) and Pluronic F-127 (0.02%, Invitrogen). The dye was loaded for 30 minutes at room temperature followed by wash and de-esterification for 30 minutes. Fluo-4 was excited at 488 nm using an Argon laser, and emission was collected using a 500-530 nm bandpass filter. Images were recorded using confocal microscopy in line scan mode (Bio-Rad Radiance 2100, Hercules, CA, USA) using a 40x objective and scanned at 6 ms/line. Intact cardiomyocytes were plated on laminin-coated coverslips and paced at 1 Hz in a field stimulation chamber (Warner Instruments, Hamden, CT, USA). Myocytes were continuously perfused with Tyrode's solution containing (in mmol/L): NaCl 140, KCl 4, CaCl<sub>2</sub> 1.8, MgCl<sub>2</sub> 1, HEPES 5, Na-HEPES 5, glucose 5.5; pH=7.40. Sarcoplasmic Ca<sup>2+</sup> content was assessed by local delivery of 10 mmol/L caffeine. ImageJ was used for image processing and analysis. During analysis, the non-cellular background fluorescence was subtracted, and the control baseline (non-paced) fluorescence (F<sub>0</sub>) was determined in each cell. There was no statistical difference in F<sub>0</sub> values between *db/db*+Aldo and WT+Vehicle myocytes.

### **Cellular electrophysiology**

Isolated single murine ventricular cardiomyocytes were placed in a temperature-controlled perfusion chamber (Warner Instruments) mounted on a Leica DMI3000 B inverted microscope (Leica Microsystems, Buffalo Grove, IL, USA). Cells were bathed at 37°C (for 10 minutes before starting the experiments) and continuously perfused (2 mL/min) with Tyrode's solution containing (in mmol/L): NaCl 140, KCl 4, CaCl<sub>2</sub> 1.8, MgCl<sub>2</sub> 1, HEPES 5, Na-HEPES 5, glucose 5.5; pH=7.40. Electrodes were fabricated from borosilicate glass (World Precision Instruments., Sarasota, FL, USA) having tip resistances of 2 to 2.5 MΩ when filled with internal solution containing (in mmol/L): K-aspartate 100, KCl 30, NaCl 8, Mg-ATP 5, phosphocreatine dipotassium salt 10, HEPES 10, EGTA 0.01, cAMP 0.002, and calmodulin 0.0001; pH=7.20 (with KOH). Using this internal solution, the intracellular Ca<sup>2+</sup> transient and contraction of the cardiomyocyte are preserved. Axopatch 200B amplifier (Axon Instruments Inc., Union City, CA, USA) was used for recordings and the signals were digitized at 50 kHz by a Digidata 1322A A/D converter (Axon Instruments) under software control (pClamp10.4). Series resistance was typically 3 to 5 MΩ and it was compensated by ≥90%. Experiments were discarded when the series resistance was high or increased by ≥20% during the recordings. Experiments were conducted at 37±0.1°C.

APs were recorded in whole-cell I-clamp conditions where cells were stimulated using supra-threshold depolarizing pulses (2 ms duration) delivered via the patch pipette at 1 Hz frequency. AP duration at 90% repolarization (APD<sub>90</sub>) was used to characterize AP repolarization. Series of 50 consecutive APs

were analyzed to estimate short-term variability (STV) of  $APD_{90}$  according to the following formula:  $STV = \frac{\sum(|APD_{n+1} - APD_n|)}{[(n_{beats} - 1) \times \sqrt{2}]}$ , where  $APD_n$  and  $APD_{n+1}$  indicate the durations of the  $n^{th}$  and  $(n+1)^{th}$  APs, and  $n_{beats}$  denotes the total number of consecutive beats analyzed. Diastolic arrhythmogenic activities were elicited by cessation of 1-min burst pacing (10 Hz), and membrane potential was recorded for additional 1 minute. Delayed afterdepolarizations (DADs) were defined as an increase in resting membrane potential exceeding 1 mV in amplitude within 0.5 seconds. Spontaneous APs (sAPs) were defined as depolarizations showing overshoot with a fast upstroke phase.

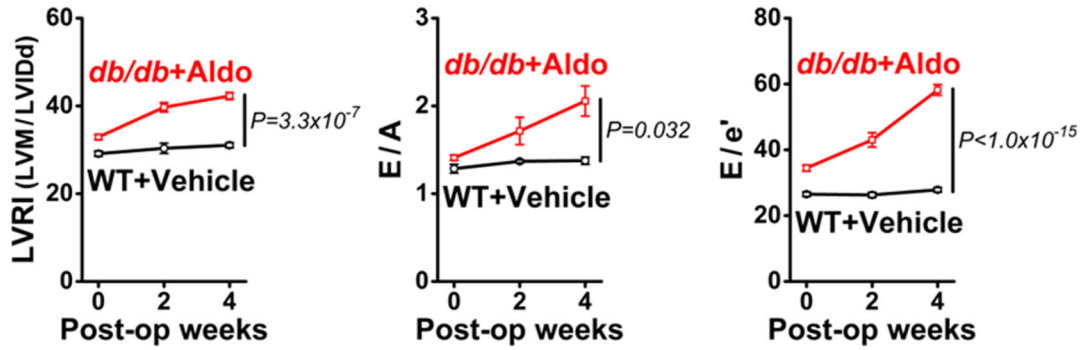
In voltage-clamp  $I_{Na,Late}$  measurements, internal solution contained (mmol/L): CsCl 110, tetraethylammonium chloride 20, Mg-ATP 5, HEPES 10, phosphocreatine disodium salt 5, calmodulin 0.0001, EGTA 10,  $CaCl_2$  4.1 (free  $[Ca^{2+}] = 100$  nmol/L), pH=7.20. Bath solution contained (mmol/L): NaCl 140, CsCl 4,  $CaCl_2$  1.8,  $MgCl_2$  1, HEPES 5, Na-HEPES 5, glucose 5.5, 4-aminopyridine 5, nifedipine 0.01, pH=7.40.  $I_{Na,Late}$  was measured at the end of a 500 ms depolarizing pulse to -40 mV from a -120 mV holding potential.  $I_{Na,Late}$  could be inhibited by tetrodotoxin (TTX, 10  $\mu$ mol/L), and the TTX-sensitive current amplitude was normalized to cell capacitance ( $I_{Na,Late}$  density) in each cell.

Chemicals and reagents were purchased from Sigma-Aldrich (St. Louis, MO, USA), if not specified otherwise. Empagliflozin was from MedChemExpress (Monmouth Junction, NJ, USA).

### Statistical analysis

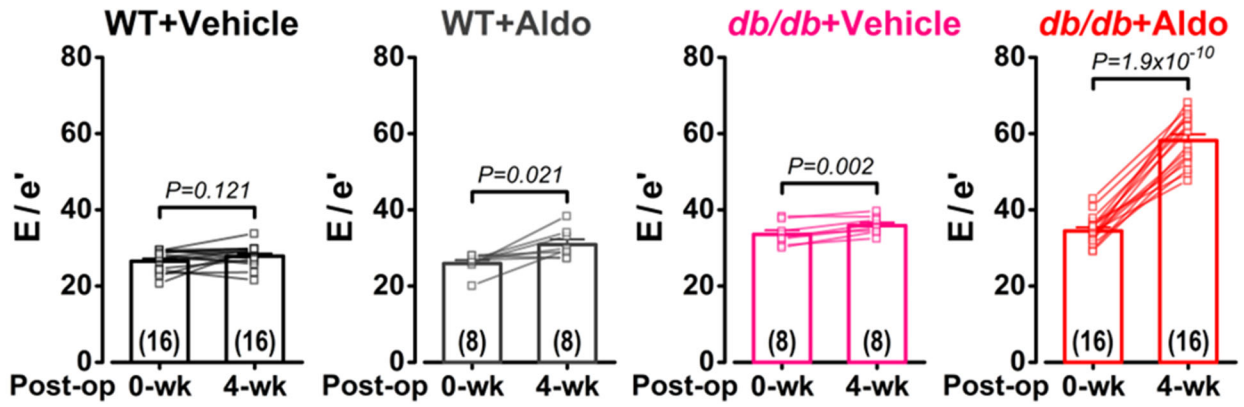
Pooled data are presented as Mean $\pm$ SEM. The number of biological and technical replicates in each experimental group is reported in the figures and figure legends. Normality of the data was assessed by Shapiro-Wilk test and the equality of group variance was tested using Brown-Forsythe test. Statistical significance of differences was determined using two-tailed *t*-test, Mann-Whitney test, and ANOVA with Tukey's or Dunn's multiple comparisons test, when applicable. Interaction between genotype and treatment was determined using two-way ANOVA. GraphPad Prism 9 (San Diego, CA, USA) software was used for data analysis. Blinded data acquisition and analysis have been performed for all *in vivo* measurements (echocardiography). Animals were grouped with no blinding but randomized in cellular experiments. Fully blinded analysis was not performed in cellular studies because the same person carried out the experiments and analysis. Male and female animals were used in equal numbers. Group sizes were determined by an a priori power analysis for a two-tailed *t*-test with an  $\alpha$  of 0.05 and power of 0.8, in order to detect a 20% difference signal at the endpoint. Origin 2016 (OriginLab, Northampton, MA, USA) software was used for plotting the data.

Figure S1. Progression of cardiac remodeling and diastolic dysfunction during aldosterone infusion



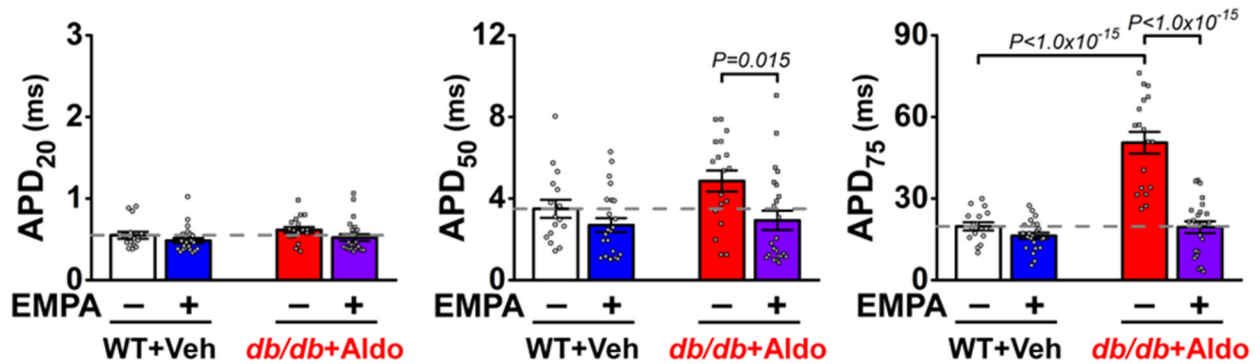
Longitudinal echocardiographic follow-up of db/db mice with chronic aldosterone infusion (db/db+Aldo) and wild-type (WT) mice with vehicle infusion (WT+Vehicle). Biweekly monitoring of left ventricular remodeling index (LVRI) and diastolic dysfunction (E/A and E/e') before and after minipump implantation. LVM, left ventricular mass; LVIDd, left ventricular end-diastolic diameter; E/A, ratio between mitral E wave and A wave; E/e', ratio between mitral E wave and e' wave. Osmotic minipumps filled with either aldosterone (0.3  $\mu\text{g}/\text{hour}$ ) or vehicle (saline with 5% ethanol) were implanted in 12-week-old mice (N=16 in each treatment group). Repeated measures mixed-effect model (REML) with Geisser-Greenhouse correction was used to calculate interaction between genotype and post-operative weeks.

Figure S2. Progression of diastolic dysfunction ( $E/e'$ ) during the 4-week study period



Paired data of  $E/e'$  (ratio between mitral E and  $e'$  waves) in Doppler echocardiography before and 4-week after aldosterone (Aldo, 0.3  $\mu\text{g}/\text{hour}$ ) or vehicle treatment via implanted osmotic minipumps in wild-type (WT) and db/db mice. Paired t-test. Animal numbers (N) are shown in the figure.

Figure S3. Action potential duration at 20%, 50%, and 75% of repolarization



Action potential duration (APD) at 20%, 50%, and 75% of repolarization (APD<sub>25</sub>, APD<sub>50</sub>, and APD<sub>75</sub>, respectively) in WT+Vehicle and db/db+Aldosterone (Aldo) myocytes without or with preincubation with empagliflozin (EMPA, 1  $\mu$ mol/L, 4 hours). Cardiomyocytes were paced at 1 Hz. Mean  $\pm$  SEM is shown. ANOVA followed by Tukey's multiple comparisons test. n = 16 cells from 7 animals in WT+Vehicle without EMPA treatment; n = 23 cells from 7 animals in WT+Vehicle with EMPA treatment; n = 18 cells from 8 animals in db/db+Aldo without EMPA treatment; and n = 23 cells from 8 animals in db/db+Aldo with EMPA treatment. Each individual myocyte is shown as a data point.